Supplementary Materials for

Sleep Releases Action-Mode Network Revealed by Human Connectome

Yang *et al.*

*Corresponding authors.

Email: yanggy@bit.edu.cn; liuhesheng@cpl.ac.cn; jgao@pku.edu.cn

This PDF file includes:

Supplementary Figures 1 to 11

Supplementary Tables 1-2

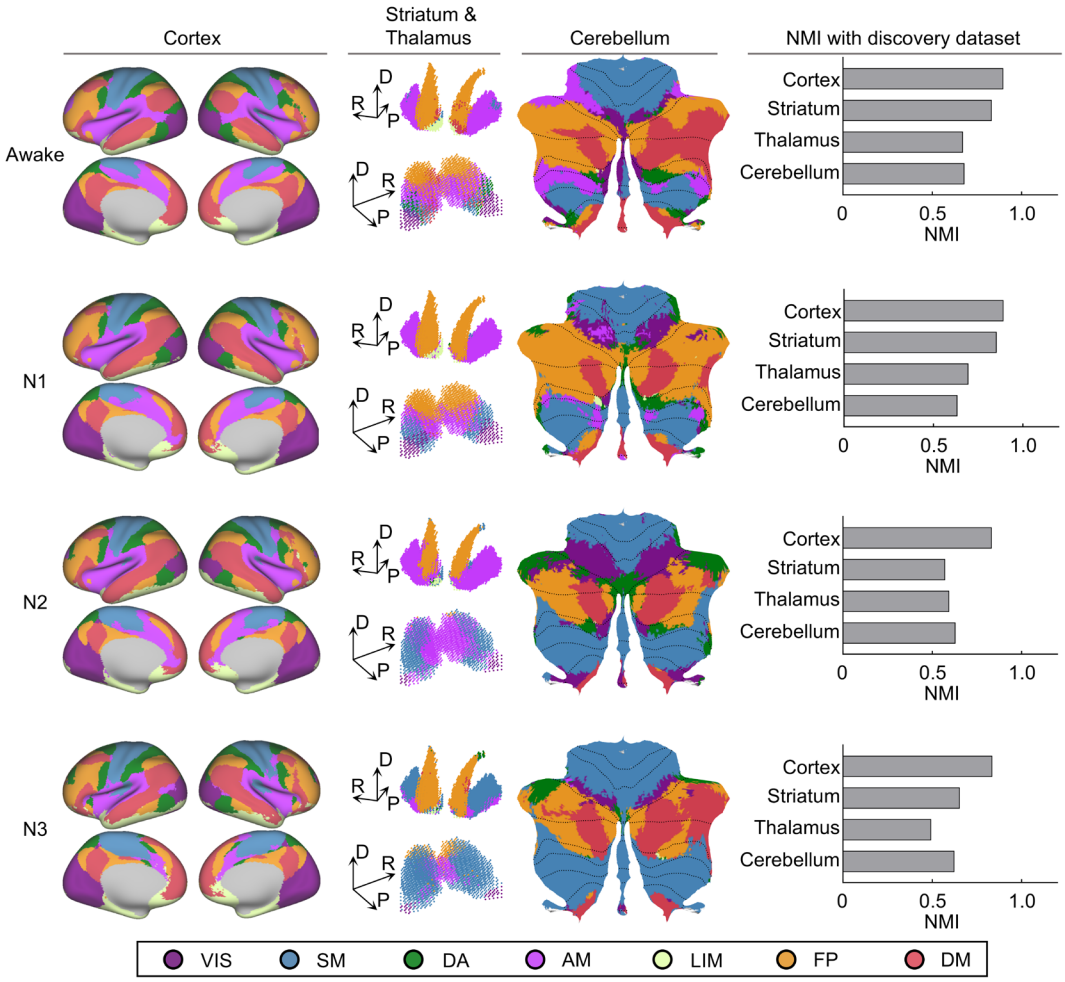

Figure S1 | The seven-network parcellations for the cerebral cortex, striatum, thalamus and cerebellum during wakefulness and sleep based on the balanced dataset. Brain parcellations were constructed in awake, N1, N2, and N3 sleep. Due to the relatively small number of REM sleep epochs after balancing, we did not include REM sleep in the balanced dataset. Overall, there was strong correspondence between the brain parcellations from the discovery and balanced datasets. Similarity was quantified using Normalized Mutual Information (NMI), a measure of the similarity between two sets of functional brain networks. VIS, visual; SM, somatomotor; DA, dorsal attention; AM, action-mode; LIM, limbic; FP, frontoparietal; DM, default-mode. REM, repaid eye movement.

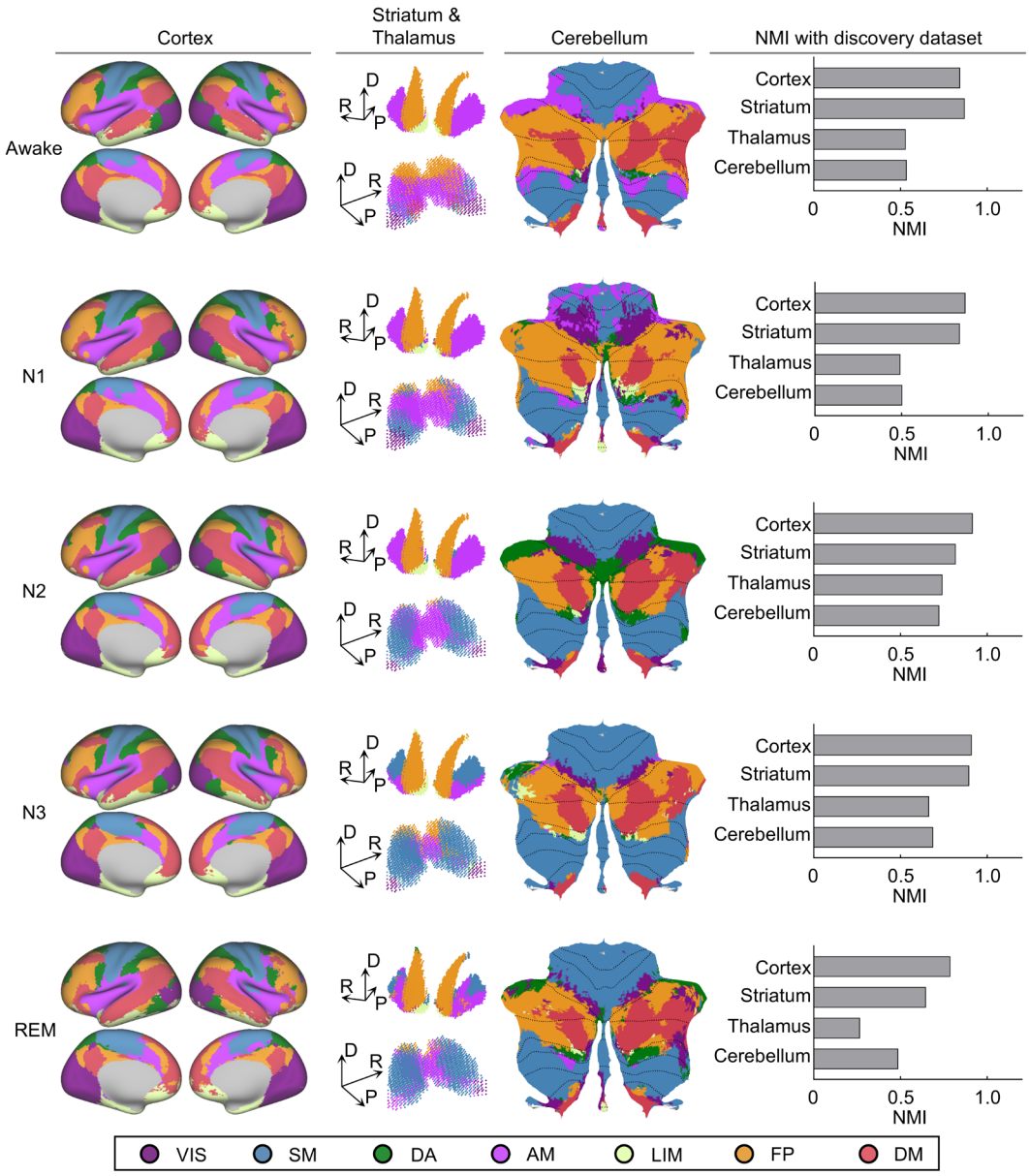

Figure S2 | The seven-network parcellations for the cerebral cortex, striatum, thalamus and cerebellum during wakefulness and sleep based on longer duration epochs (8-minute) from the EEG-fMRI dataset. Parcellations for the brain were constructed for awake, N1, N2, N3, and REM sleep states. Overall, there was strong correspondence between the discovery and longer duration epoch datasets of the parcellations. Similarity was quantified using NMI.

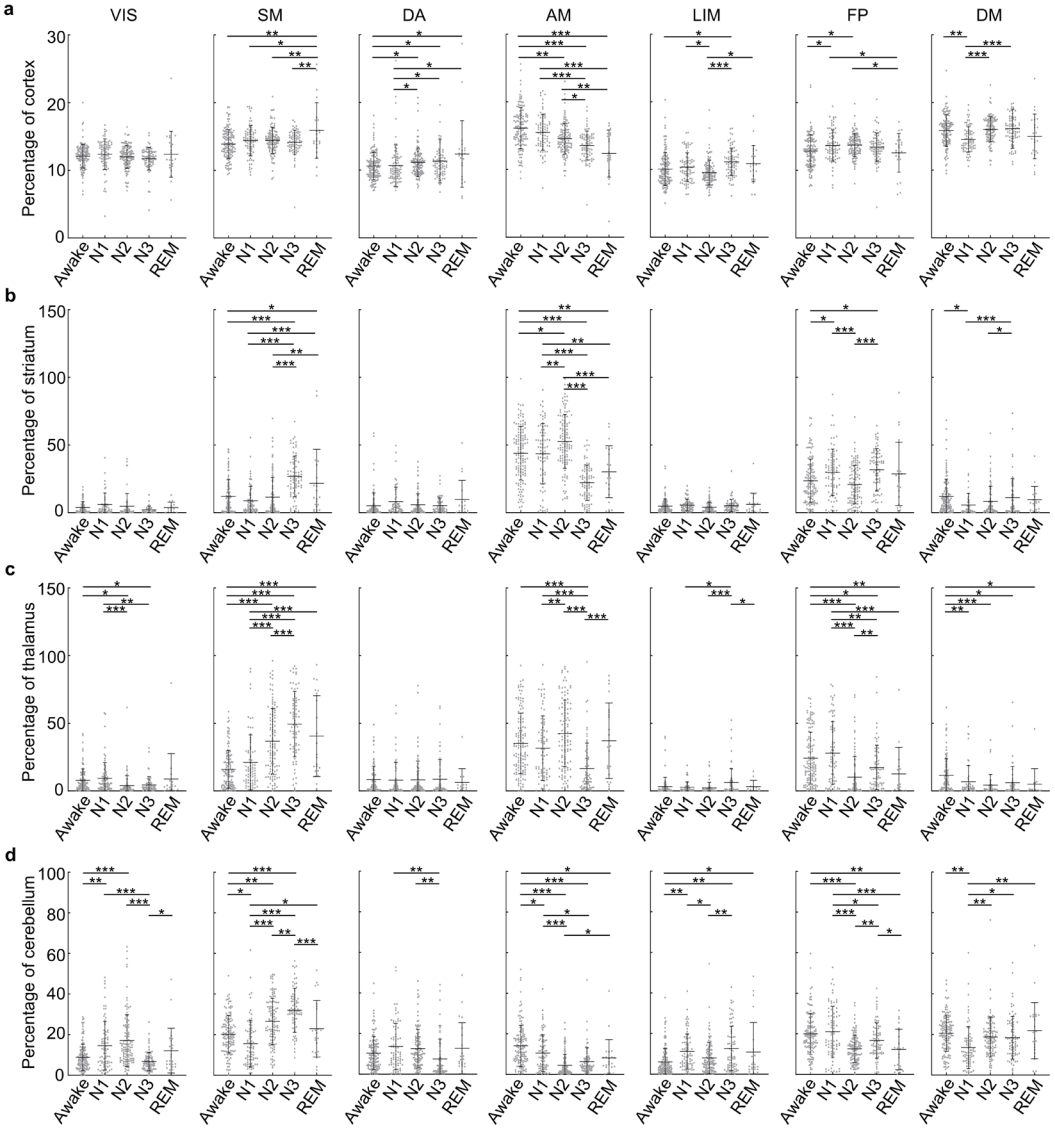

Figure S3 | The individualized percentage of each network across the cerebral cortex and subcortical structures changed significantly during sleep in the discovery dataset. The percentage of each network's total cortical surface area and subcortical volume was quantified separately for the cerebral cortex (**a**), striatum (**b**), thalamus (**c**), and cerebellum (**d**). The main effect of sleep stage on the percentage of each network on cerebral cortex and subcortical structures was evaluated using linear mixed-effect (LME) modeling (please see the Methods for more details). For the cortex, significant main effects of sleep stage were found for the percentage of network area in the somatomotor ($\chi^2(4) = 14.54$, $P = 0.006$), dorsal attention ($\chi^2(4) = 17.62$, $P = 0.002$), action-mode ($\chi^2(4) = 50.54$, $P < 0.001$), limbic ($\chi^2(4) = 30.81$, $P < 0.001$), frontoparietal ($\chi^2(4) = 18.03$, $P = 0.002$), and default-mode ($\chi^2(4) = 29.73$, $P < 0.001$) networks. For the striatum, significant effects were observed in the somatomotor ($\chi^2(4) = 94.54$, $P < 0.001$), action-mode ($\chi^2(4) = 138.44$, $P < 0.001$), frontoparietal ($\chi^2(4) = 34.22$, $P < 0.001$), and default-mode ($\chi^2(4) = 20.93$, $P < 0.001$) networks. For the thalamus, significant effects were found in the visual ($\chi^2(4) = 24.18$, $P < 0.001$), somatomotor ($\chi^2(4) = 77.02$, $P < 0.001$), action-mode ($\chi^2(4) = 73.78$, $P < 0.001$), limbic ($\chi^2(4) = 19.79$, $P < 0.001$), frontoparietal ($\chi^2(4) = 75.64$, $P < 0.001$), and default-mode ($\chi^2(4) = 31.04$, $P < 0.001$) networks. For the cerebellum, significant main effects were found in the visual ($\chi^2(4) = 84.67$, $P < 0.001$), somatomotor ($\chi^2(4) = 119.22$, $P < 0.001$), dorsal attention ($\chi^2(4) = 21.43$, $P < 0.001$), action-mode ($\chi^2(4) = 102.81$, $P < 0.001$), limbic ($\chi^2(4) = 33.52$, $P < 0.001$),

frontoparietal ($\chi^2(4) = 58.44$, $P < 0.001$), and default-mode ($\chi^2(4) = 27.51$, $P < 0.001$) networks. *$P < 0.05$, **$P < 0.01$, ***$P < 0.001$. All P values are corrected for multiple comparison for the cerebral cortex and subcortical structures across networks using the False Discover Rate (FDR) with $q < 0.05$. Points represent, for each participant, the proportion of voxels assigned to a given network within each brain region. Data are presented as mean ± s.d.

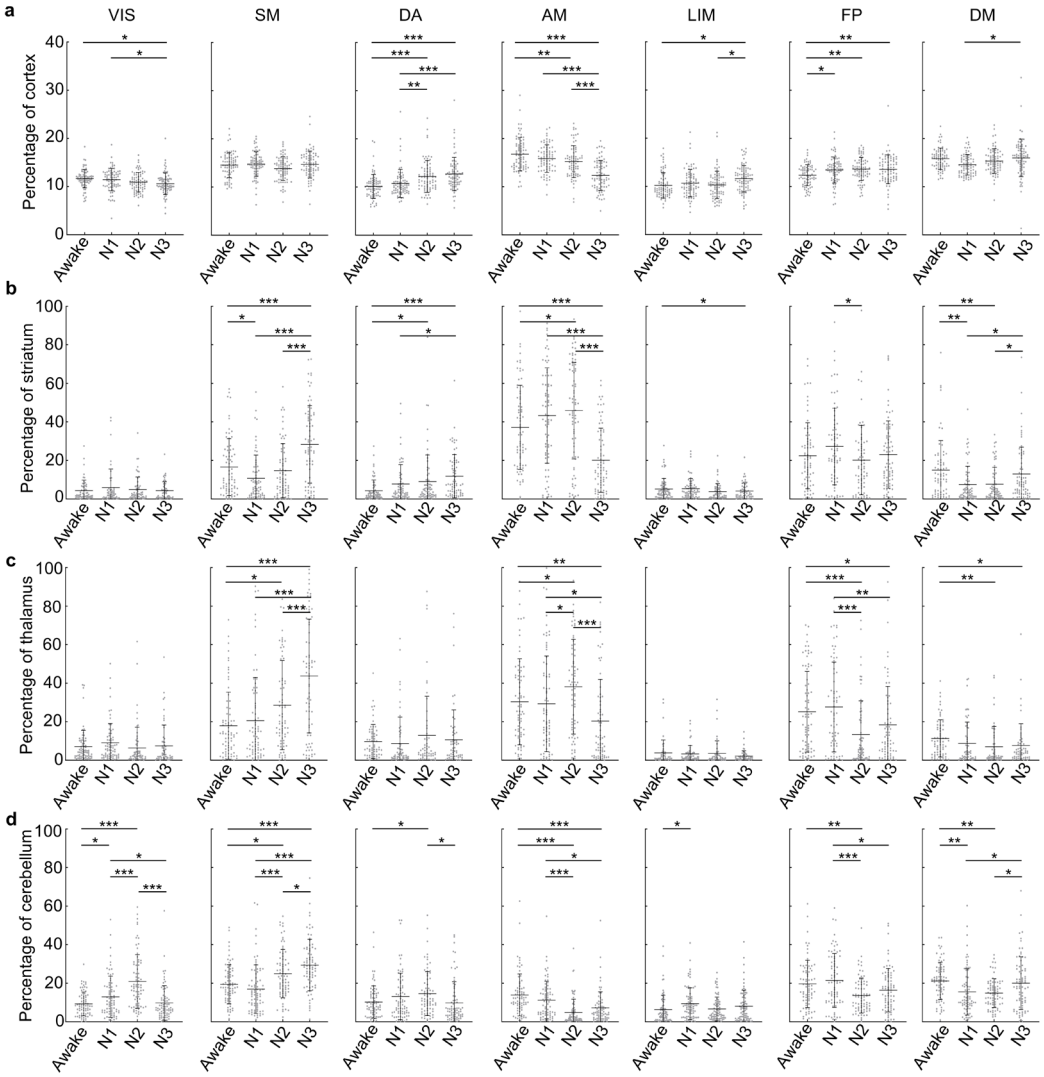

Figure S4 | The individualized percentage of each network across the cerebral cortex and subcortical structures changed significantly during sleep in the balanced dataset. The percentage of each network's total cortical surface area and subcortical volume was quantified separately for the cerebral cortex (**a**), striatum (**b**), thalamus (**c**), and cerebellum (**d**). The main effect of sleep stage on the percentage of each network was estimated with LME modeling. For the cortex, significant main effects of sleep stage were found for the percentage of network area in the visual ($\chi^2(3) = 12.45$, $P = 0.008$), dorsal attention ($\chi^2(3) = 38.50$, $P < 0.001$), action-mode ($\chi^2(3) = 81.99$, $P < 0.001$), limbic ($\chi^2(3) = 12.31$, $P = 0.008$), frontoparietal ($\chi^2(3) = 12.56$, $P = 0.008$), and default-mode ($\chi^2(3) = 12.56$, $P = 0.008$) networks. For the striatum, significant main effects were found in the somatomotor ($\chi^2(3) = 62.15$, $P < 0.001$), dorsal attnetion ($\chi^2(3) = 22.84$, $P < 0.001$, action-mode ($\chi^2(3) = 63.57$, $P < 0.001$), limbic ($\chi^2(3) = 10.22$, $P = 0.023$), and default-mode ($\chi^2(3) = 19.20$, $P < 0.001$) networks. For the thalamus, significant main effects were found in the somatomotor ($\chi^2(3) = 50.95$, $P < 0.001$), action-mode ($\chi^2(3) = 28.45$, $P < 0.001$), frontoparietal ($\chi^2(3) = 26.98$, $P < 0.001$), and default-mode ($\chi^2(3) = 11.24$, $P = 0.018$) networks. For the cerebellum, significant main effects were found in the visual ($\chi^2(3) = 65.58$, $P < 0.001$), somatomotor ($\chi^2(3) = 48.77$, $P < 0.001$), dorsal attention ($\chi^2(3) = 10.38$, $P = 0.018$), action-mode ($\chi^2(3) = 47.60$, $P < 0.001$), limbic ($\chi^2(3) = 8.81$, $P = 0.032$), frontoparietal ($\chi^2(3) = 19.47$, $P < 0.001$), and default-mode ($\chi^2(3) = 18.05$, $P < 0.001$) networks. *$P < 0.05$, **$P < 0.01$, ***$P < 0.001$. All P values are corrected for multiple comparison for cerebral cortex and subcortical structures across networks using

FDR with $q < 0.05$. Points represent, for each participant, the proportion of voxels assigned to a given network within each brain region. Data are presented as mean ± s.d.

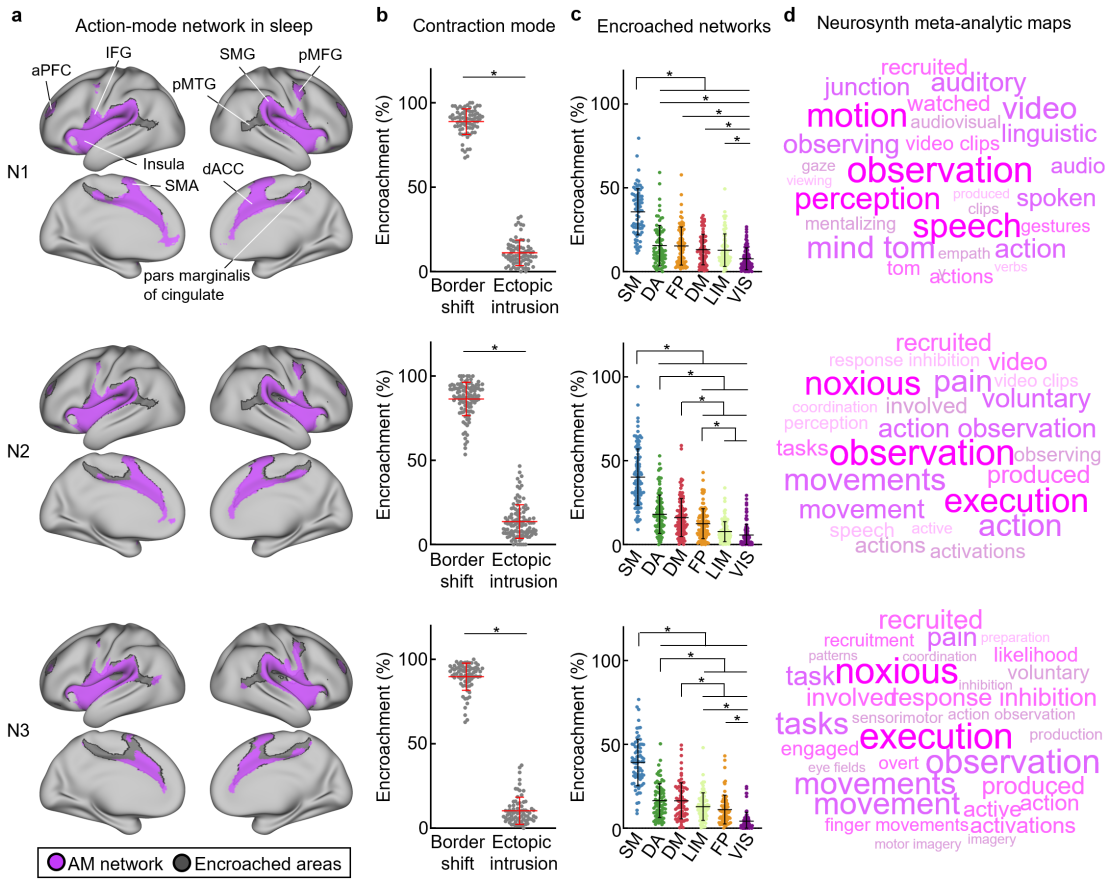

Figure S5 | Contraction of the action-mode network during sleep in cerebral cortex. a, Group-level action-mode networks in N1, N2, and N3 sleep are displayed in purple. Gray areas indicate regions where the wakefulness action-mode network was encroached upon during sleep. These regions are primarily located in the posterior middle temporal gyrus (pMTG), anterior prefrontal cortex (aPFC), supplementary motor area (SMA), posterior middle frontal gyrus (pMFG), and pars marginalis of cingulate. **b**, The contraction of the action-mode network is primarily due to border shifts rather than ectopic intrusions (defined as isolated patches of the network in atypical locations; two-sided paired sample *t*-test, $^*P < 0.0001$; N1: $n = 78$, N2: $n = 111$, N3: $n = 77$, adjusted for multiple comparisons with FDR q < 0.05). Data points indicate subject number. Data are presented as mean ± s.d. **c**, The action-mode network is encroached upon by different functional networks in sleep. A linear mixed-effects model revealed a main effect of network identity across all sleep stages (N1: $\chi^2(5) = 476.77$, $P < 0.0001$; N2: $\chi^2(5) = 1336.50$, $P < 0.0001$; N3: $\chi^2(5) = 886.18$, $P < 0.0001$). Asterisks represent statistical significance in post hoc two-sided paired sample *t*-test ($P < 0.001$, adjusted for multiple comparisons with FDR q < 0.05). Data point denotes the subject number (N1: $n = 78$, N2: $n = 111$, N3: $n = 77$). Data are presented as mean ± s.d. **d**, In light sleep (N1 and N2), the encroached area of the action-mode network showed the strongest convergence with Neurosynth meta-analytic maps for observation functions. In deep sleep (N3), it was most strongly associated with maps for execution functions. IFG, inferior frontal gyrus; SMG, supramarginal gyrus; dACC, dorsal anterior cingulate cortex.

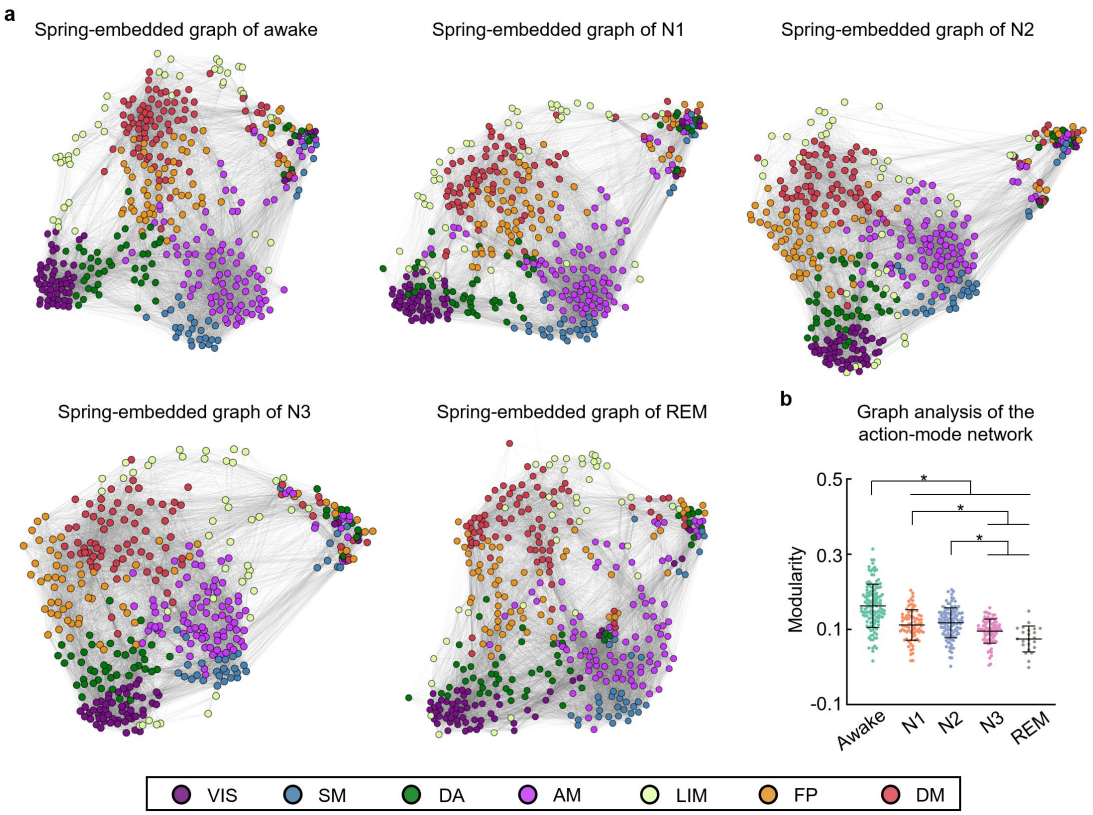

Figure S6 | Sleep promotes the integration of the action-mode network with the whole-brain. a, Spring-embedded plots visualize group-average networks, where well-connected groups of nodes are pulled together. During wakefulness, the action-mode network is closely connected with the somatomotor, dorsal attention, and frontoparietal networks, while keeping distance from the default-mode network, forming a two-pole structure. As sleep deepens, the action-mode network is gradually encroached upon by the somatomotor network and moves closer to the dorsal attention and default-mode networks. **b**, Modularity quantifies the individualized degree of association between the action-mode network and the rest of other networks. The main effect of sleep stage on modularity of the action-mode network was estimated using LME modeling. We found a significant main effect of sleep stage on the modularity of the action-mode network in relation to other networks ($\chi^2(4) = 355.03$, $P < 0.001$). Asterisks indicate statistical significance in post hoc two-sided two-sample *t*-test ($P < 0.05$, corrected for multiple comparison using FDR with $q < 0.05$). The sample size for awake, N1, N2, N3, REM states (i.e. the modularity of each participant) are 128, 78, 111, 77 and 23, respectively. Data are presented as mean ± s.d.

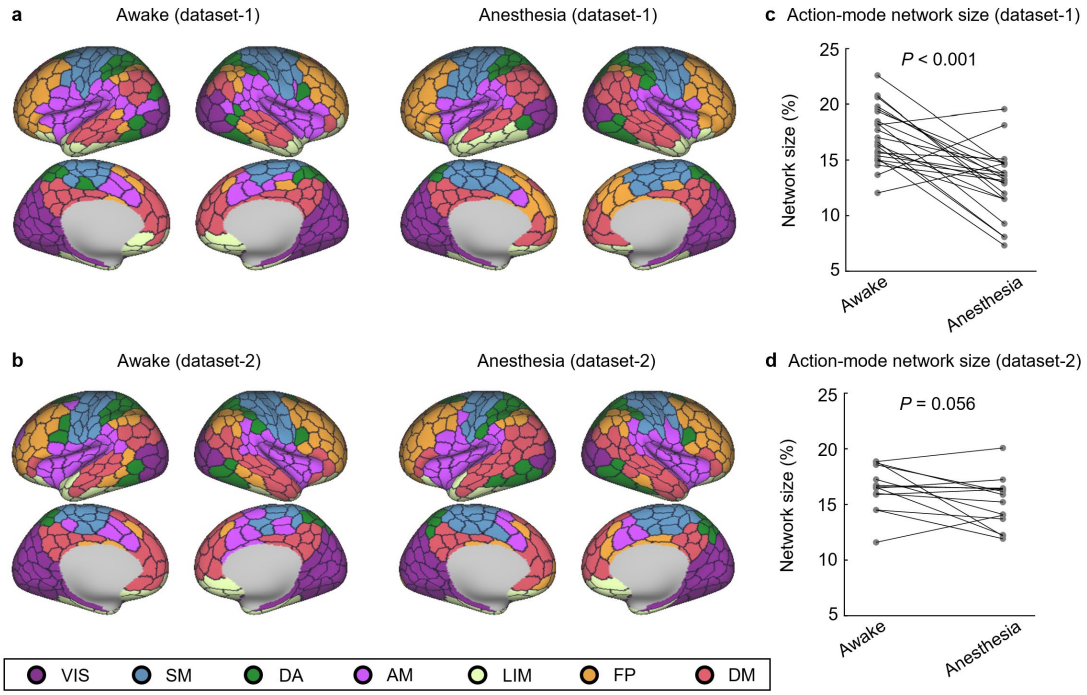

Figure S7 | The seven-network parcellations for the cerebral cortex during wakefulness and anesthesia were analyzed using two human anesthesia datasets. a, The group-level parcellations of the cortex for dataset-1, comparing awake and anesthetized states, showed that the action-mode network contracted during anesthesia relative to wakefulness. **b**, In dataset-2, the group-level brain parcellations between awake and anesthetized states similarly validated the contraction of the action-mode network observed in dataset-1. **c**, The contraction in network size between wakefulness and anesthesia was significantly different in individualized cortical parcellations in dataset-1 (two-sided paired sample *t*-test, $P < 0.001$). Points represent individual-level network size of the action-mode network in the awake and anesthesia stages ($n = 23$). **d**, In dataset-2, while the action-mode network did not show a statistically significant difference between wakefulness and anesthesia, a trend toward contraction was still observed (two-sided paired sample *t*-test, $P = 0.056$). Points represent individual-level network size of the action-mode network in the awake and anesthesia stages ($n = 14$).

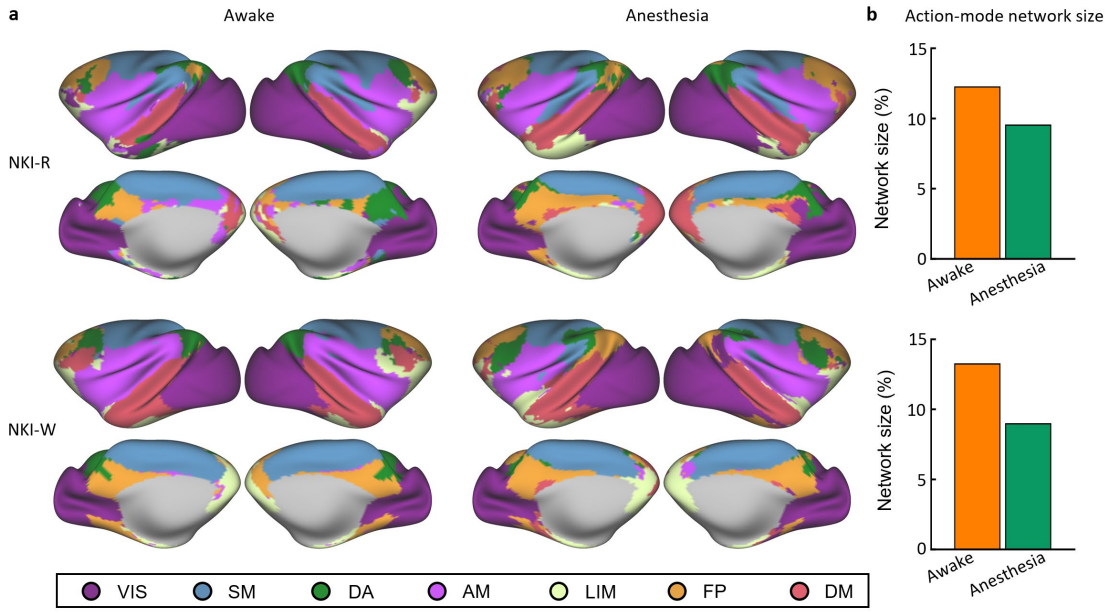

Figure S8 | The seven-network parcellations of the cerebral cortex during wakefulness and anesthesia were analyzed based on two macaques. a, The individualized cortical parcellations for macaques NKI-R and NKI-W were constructed in both awake and anesthetized states. Visual inspection revealed a notable contraction in the action-mode network for each subject, primarily due to encroachment by the somatomotor network within the insula cortex. **b**, Quantitative analysis showed that the size of the action-mode network in NKI-R decreased from 12% during wakefulness to 9% under anesthesia, while in NKI-W, it decreased from 13% during wakefulness to 9% under anesthesia.

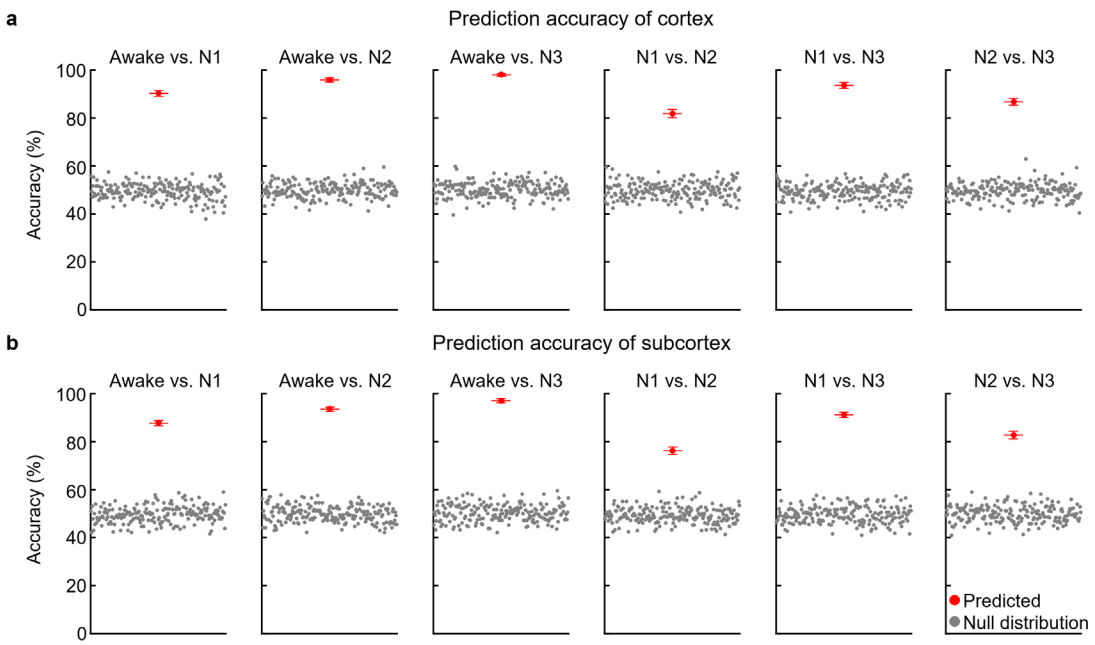

Figure S9 | Binary machine learning classifiers accurately distinguish each pair of sleep stages based on the functional network topology of the cerebral cortex and subcortical structures. a, The binary classification results between all sleep stages indicated that the binary SVM classifiers were able to identify sleep stages above chance level for each pair of sleep stages using the functional network topology of the cerebral cortex as features (awake vs. N1: accuracy 90.4%, $P < 0.05$; awake vs. N2: accuracy 96.0%, $P < 0.05$; awake vs. N3: accuracy 98.2%, $P < 0.05$; N1 vs. N2: accuracy 81.8%, $P < 0.05$; N1 vs. N3: accuracy 93.7%, $P < 0.05$; N2 vs. N3: accuracy 96.8%, $P < 0.05$). **b**, Binary classifiers could also accurately distinguish sleep stages using the functional network topology of subcortical structures as features (awake vs. N1: accuracy 87.9%, $P < 0.05$; awake vs. N2: accuracy 93.7%, $P < 0.05$; awake vs. N3: accuracy 97.1%, $P < 0.05$; N1 vs. N2: accuracy 76.2%, $P < 0.05$; N1 vs. N3: accuracy 91.1%, $P < 0.05$; N2 vs. N3: accuracy 82.7%, $P < 0.05$). Significance was assessed using a permutation test adjusted for multiple comparisons with FDR $q < 0.05$. Red points indicate mean classification accuracy (5-fold cross-validation with $n = 100$); grey points represent a null distribution (5-fold cross-validation with $n = 200$). Data are presented as mean ± s.d.

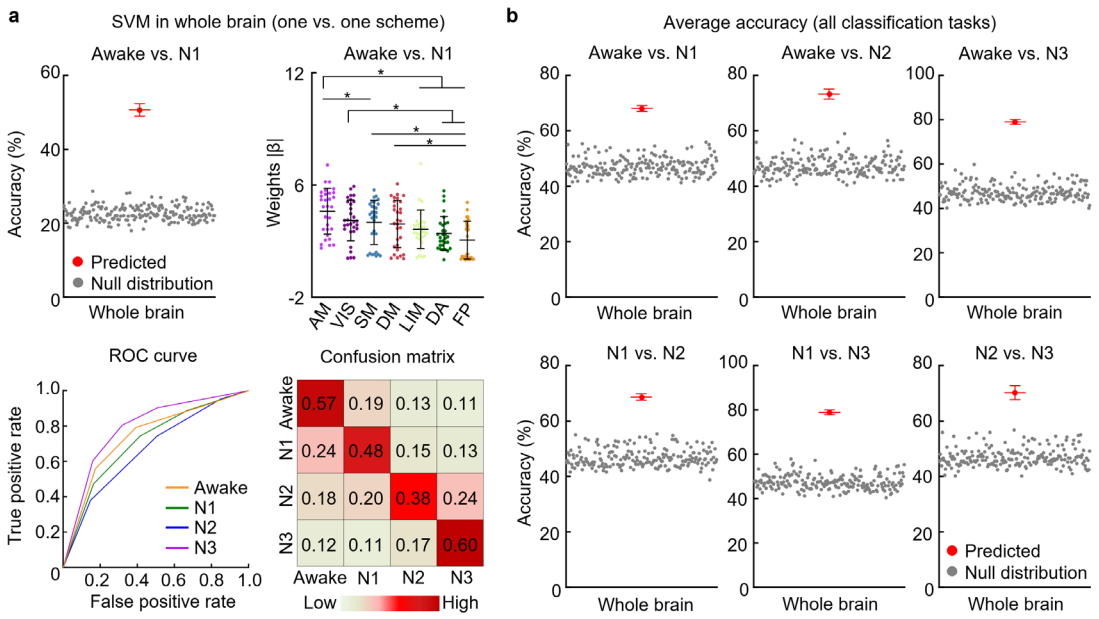

Figure S10 | The machine learning classifier accurately distinguishes sleep stages based on the size of functional networks across the whole brain. a, The probability of correctly identifying different NREM sleep stages with the Support Vector Machine (SVM) classifier under a one-against-one scheme was above chance (accuracy 50.6%, significance assessed using a permutation test, $P < 0.05$) when using the size of each functional network in the whole brain as features. The linear predictor weights (β) showed a significant difference between the contributions of different networks, with the action-mode network contributing the most to the prediction. Asterisks represent statistical significance in two-sided paired sample *t*-test ($P < 0.001$, adjusted for multiple comparisons with FDR $q < 0.05$). Receiver operating characteristic (ROC) curve and confusion matrix demonstrate the performance of multiclass SVM classifier. **b**, The binary classification results between all sleep stages showed that the SVM classifier could identify sleep stages above chance (awake vs. N1: accuracy 67.9%, $P < 0.05$; awake vs. N2: accuracy 73.2%, $P < 0.05$; awake vs. N3: accuracy 78.9%, $P < 0.05$; N1 vs. N2: accuracy 68.5%, $P < 0.05$; N1 vs. N3: accuracy 78.8%, $P < 0.05$; N2 vs. N3: accuracy 70.2%, $P < 0.05$). Significance was assessed using a permutation test adjusted for multiple comparisons with FDR $q < 0.05$. Red points indicate mean classification accuracy (5-fold cross-validation with $n = 100$); grey points represent a null distribution (5-fold cross-validation with $n = 200$). Points of weight (β) for each network were calculated from the linear SVM classifier (5 times repeated sampling with 6 one-against-one classifiers, resulting in 30 final values). Data are presented as mean ± s.d.

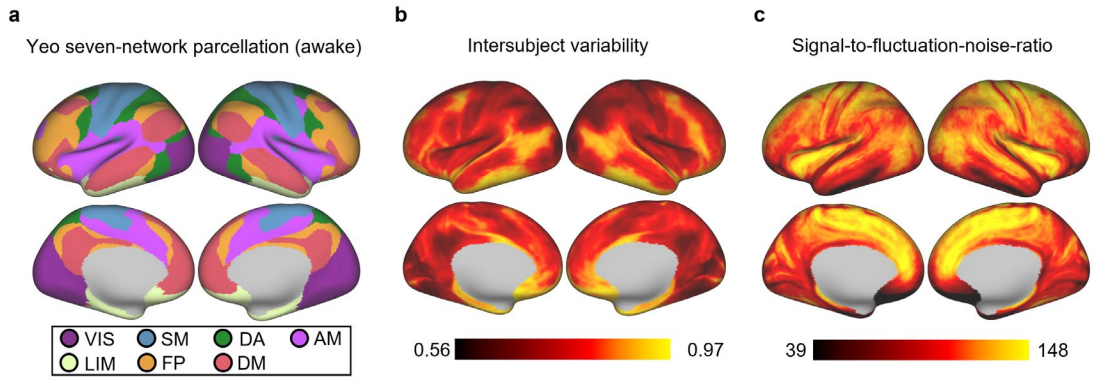

Figure S11 | The initial Yeo seven-network parcellation, intersubject variability, and signal-to-fluctuation-noise-ratio maps were constructed using fMRI data acquired during wakefulness. a, The initial population-based functional parcellation was generated from eyes-open resting-state fMRI data using a clustering algorithm based on the von Mises–Fisher distribution. In this procedure, 59,412 cortical surface vertices were first randomly assigned to different networks and then iteratively reassigned to network memberships to maximize the similarity of connectivity profiles among vertices within the same network. This seven-network parcellation served as the initialization for the subsequent iterative search algorithm used to derive individualized cortical parcellations. **b**, Intersubject variability in functional connectivity was quantified using repeated eyes-open resting-state fMRI measurements, providing an estimate of between-subject variability in connectivity patterns. **c**, Cortical signal-to-fluctuation-noise ratio (SFNR) was computed from eyes-open resting-state fMRI data and was used as a weighting factor during the subcortical parcellation process.

Supplementary Table 1 | Demographic information and head motion values of the balanced EEG-fMRI dataset.

Sleep stage	Number of subject	Female (%)	Age range in years (mean ± SD)	Number of fMRI epoch	FD (mean ± SD)	DVARS (mean ± SD)
Awake	76	43 (56.6%)	18~35 (22.6 ± 3.7)	76	0.11 ± 0.03	20.72 ± 2.95
N1	76	49 (64.5%)	18~36 (22.3 ± 3.5)	76	0.11 ± 0.04	21.23 ± 4.03
N2	76	48 (63.2%)	18~29 (22.3 ± 2.9)	76	0.12 ± 0.04	22.01 ± 4.05
N3	76	47 (61.8%)	18~30 (21.9 ± 3.2)	76	0.12 ± 0.04	22.85 ± 4.58

Supplementary Table 2 | Demographic information and head motion values for the 8-minute EEG-fMRI epochs.

Sleep stage	Number of subject	Female (%)	Age range in years (mean ± SD)	Number of fMRI epoch	FD (mean ± SD)	DVARS (mean ± SD)
Awake	74	38 (51.4%)	18~36 (22.64 ± 4.00)	241	0.21 ± 0.15	25.40 ± 6.22
N1	40	23 (57.5%)	18~36 (22.67 ± 3.88)	54	0.12 ± 0.05	21.68 ± 3.55
N2	88	51 (57.9%)	18~36 (22.60 ± 3.86)	401	0.13 ± 0.05	22.52 ± 4.28
N3	66	42 (63.6%)	18~29 (21.30 ± 2.91)	278	0.12 ± 0.04	23.24 ± 4.44
REM	16	11 (68.8%)	19~30 (22.75 ± 3.44)	38	0.10 ± 0.04	19.74 ± 2.68